

Article

Critical Role of Al Pair Sites in Methane Oxidation to Methanol on Cu-Exchanged Mordenite Zeolites

Peijie Han ¹, Zhaoxia Zhang ¹, Zheng Chen ¹, Jingdong Lin ¹ , Shaolong Wan ¹, Yong Wang ² 
and Shuai Wang ^{1,*} 

- ¹ State Key Laboratory for Physical Chemistry of Solid Surfaces, Collaborative Innovation Center of Chemistry for Energy Materials, National Engineering Laboratory for Green Chemical Productions of Alcohols-Ethers-Esters, and College of Chemistry and Chemical Engineering, Xiamen University, Xiamen 361005, China; happyj@stu.xmu.edu.cn (P.H.); zzyxyy@xmu.edu.cn (Z.Z.); chenzheng@stu.xmu.edu.cn (Z.C.); jdlin@xmu.edu.cn (J.L.); swan@xmu.edu.cn (S.W.)
- ² Voiland School of Chemical Engineering and Bioengineering, Washington State University, Pullman, WA 99164, USA; wang42@wsu.edu
- * Correspondence: shuaiwang@xmu.edu.cn

Abstract: Cu-exchanged aluminosilicate zeolites have been intensively studied for the selective oxidation of methane to methanol via a chemical looping manner, while the nature of active Cu-oxo species for these catalysts is still under debate. This study inquired into the effects of Al distribution on methane oxidation over Cu-exchanged aluminosilicate zeolites, which provided an effective way to discern the activity difference between mononuclear and polynuclear Cu-oxo species. Specifically, conventional Na⁺/Co²⁺ ion-exchange methods were applied to quantify isolated Al and Al pair (i.e., Al–OH–(Si–O)_{1–3}–Al–OH) sites for three mordenite (MOR) zeolites, and a correlation was established between the reactivity of the resultant Cu-MOR catalysts and the portions of the accessible framework Al sites. These results indicated that the Cu-oxo clusters derived from the Al pair sites were more reactive than the CuOH species grafted at the isolated Al sites, which is consistent with in situ ultraviolet-visible spectroscopic characterization and density functional theory calculations. Further theoretical analysis of the first C–H bond cleavage in methane on these Cu-oxo species unveiled that stabilization of the formed methyl group was the predominant factor in determining the reactivity of methane oxidation.

Keywords: methane oxidation; methanol; mordenite zeolite; Cu-oxo species; Al pair site; C–H activation



Citation: Han, P.; Zhang, Z.; Chen, Z.; Lin, J.; Wan, S.; Wang, Y.; Wang, S. Critical Role of Al Pair Sites in Methane Oxidation to Methanol on Cu-Exchanged Mordenite Zeolites. *Catalysts* **2021**, *11*, 751. <https://doi.org/10.3390/catal11060751>

Academic Editor:
Wladimir Reschetilowski

Received: 31 May 2021
Accepted: 17 June 2021
Published: 19 June 2021

Publisher's Note: MDPI stays neutral with regard to jurisdictional claims in published maps and institutional affiliations.



Copyright: © 2021 by the authors. Licensee MDPI, Basel, Switzerland. This article is an open access article distributed under the terms and conditions of the Creative Commons Attribution (CC BY) license (<https://creativecommons.org/licenses/by/4.0/>).

1. Introduction

Methane is a major ingredient of many earth-abundant carbon resources (e.g., natural gas, combustible ice, and shale gas) [1–3]. On one hand, due to its chemical inertness brought forth by the highly stable and very weakly polarized C–H bonds (with the first C–H bond dissociation enthalpy up to ≈ 435 kJ mol^{−1}), methane is mainly used as a simple gaseous fuel to provide thermal power at present. On the other hand, it is of great interest to realize an efficient conversion of methane to valuable liquid fuels or chemicals, considering that methane itself is difficult to store and transport compared to conventional liquid fuels. In recent years, the selective oxidation of methane to C₁ platform molecules (such as CH₃OH and HCHO) has attracted much attention [4–7]. Since CH₃OH and HCHO are more reactive than the methane reactant and tend to be further oxidized to thermodynamically more stable products (i.e., CO and CO₂), the major challenge is to achieve a high selectivity of CH₃OH/HCHO at practical methane conversions. Consequently, the primary focus in this research area has been aiming at exploring novel catalysts that can enable methane oxidation under milder conditions and thus suppress the undesired over-oxidation reactions.

In recent years, a new catalytic approach for the partial oxidation of methane to methanol on copper-exchanged aluminosilicate zeolites (Cu-zeolite for short) has been intensively explored [7–12], which was inspired by methane monooxygenase (MMO) [13]. MMO is a biological enzyme present in microorganisms that can directly catalyze methane oxidation to methanol at ambient temperature and pressure with the Cu or Fe-oxo clusters acting as the active center. Methane oxidation on Cu-zeolites is generally carried out in a stepwise manner (so-called “chemical looping”), in which the Cu-based catalysts are first activated in an oxidative environment at high temperature (>673 K) and then used to oxidize methane to form bound methoxy species at much lower temperature (<523 K), which is followed by the hydrolysis of these methoxy species to methanol to complete the cycle. With this “chemical looping” strategy, Cu-oxo species constructed within the micropores of aluminosilicate zeolites (such as Cu-MOR [14–21], Cu-MFI [15,22,23], and Cu-CHA [24]) are shown to exhibit high methanol selectivities in the direct oxidation of methane (>80%) with the methanol yields of up to 200 $\mu\text{mol g}_{\text{cat}}^{-1}$ per cycle [12].

Although great efforts have been made in developing new Cu-zeolites for selective methane oxidation, the nature of active sites involved in these Cu-based catalysts is still under debate. For instance, at least five types of Cu-oxo species (e.g., $[\text{CuOH}]^+$ [21,25,26], $[\text{Cu}_2\text{O}]^{2+}$ [21,27], $[\text{Cu}_2\text{O}_2]^{2+}$ [15], $[\text{Cu}_3\text{O}_3]^{2+}$ [17,27], and $[\text{Cu}_5\text{O}_5]^{2+}$ [28]) have been proposed as the active sites of the Cu-MOR catalysts. The uncertainty is in part due to the fact that the formation of Cu-containing species grafted at the framework Al sites is sensitive to the Al distribution of the parent zeolite host, which varies among zeolite samples synthesized via different methods or conditions [29–33]. In general, the CuOH species prefer to bind to isolated Al sites in the zeolite framework, while the presence of multinuclear Cu-oxo species requires the presence of vicinal framework Al sites (known as Al pair sites). However, not much attention has been paid to the correlation between the Al distribution of the zeolite host and the reactivity of the resultant Cu-containing species [12], which is critical to discern the active sites for methane activation.

This study attempted to unveil the requirement of Al distribution for the reactivity of Cu-zeolite catalysts in methane oxidation to methanol and gain an insight into the origin of activity difference among the Cu-oxo species formed. To achieve these goals, this study focused on the Cu-MOR catalysts, which are among the most active ones for methane oxidation reported in the literature [12]. Three commercial H-MOR zeolite samples were selected here as the hosts of Cu-oxo species, because they possessed distinct Al distributions for the accessible framework Al sites as quantified by the $\text{Na}^+/\text{Co}^{2+}$ ion-exchange methods. The effects of Cu loading on the activity of Cu-MOR catalysts in methane oxidation to methanol revealed that the Cu-containing species formed at low Cu loadings were the predominant active sites for methane activation, which plausibly resided within the eight-member-ring channels of the MOR structure. Combined in situ ultraviolet-visible spectroscopy and density functional theory treatments indicated that both CuOH species grafted at the isolated Al sites and Cu-oxo clusters grafted at the Al pair sites (e.g., Cu_2O_2 or Cu_3O_3) were formed at the low Cu loadings, while the latter was more reactive, as they can more efficiently stabilize the methyl intermediate via bridged-O ($\mu\text{-O}$) centers. These findings shed light on the importance of Al distribution in determining the reactivity of Cu-zeolite catalysts, contributing to a fundamental guidance of the rational design of Cu-zeolite catalysts for the methane-to-methanol process.

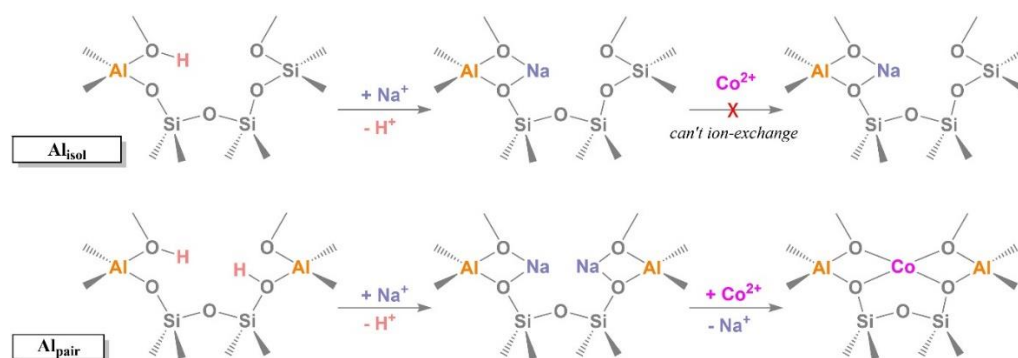
2. Results and Discussion

2.1. Preparation and Characterization of Cu-MOR Catalysts

In order to investigate the effects of Al distribution on the activity of Cu-exchanged mordenite zeolites (denoted as Cu-MOR) for methane partial oxidation to methanol, three commercial H-MOR samples with different Si/Al molar ratios (14–40; provided by the suppliers) were selected as the parent zeolite hosts, which are named henceforth as MOR-A (Si/Al = 14), MOR-B (Si/Al = 20), and MOR-C (Si/Al = 40), respectively. Since the charge induced by the isomorphous substitution of Al atoms into the SiO_4 tetrahedra units of

the zeolite framework is balanced by exchangeable proton sites, $\text{Na}^+/\text{Co}^{2+}$ ion-exchange methods were applied here to assess the components of Al sites in these H-MOR samples that are available for grafting the Cu-containing species. As illustrated in Scheme 1, Na^+ cations can replace the protons associated with the accessible framework Al sites (denoted as Al_{acce}) with a stoichiometric ratio of 1:1, while Co^{2+} cations can selectively replace the protons derived from paired Al sites (denoted as Al_{pair}) within the Al_{acce} sites [17,29–33], which are defined for two neighboring framework Al sites separated by less than three Si atoms in the ring structures of MOR (i.e., $\text{Al}-\text{OH}-(\text{Si}-\text{O})_{1-3}-\text{Al}-\text{OH}$). It needs to be noted that the two protons derived from one pair of Al sites could also be replaced by two Co^{2+} cations (corresponding to a stoichiometric Co/Al ratio of 1/1), but its occurrence requires a higher ion-exchange temperature (e.g., 350 K) [34]. In other words, the Co^{2+} -exchange process carried out at ambient temperature (c.a. 298 K) in our study enables a selective replacement of the two protons of one pair of Al sites by one Co^{2+} cation (corresponding to a stoichiometric Co/Al ratio of 1/2). Consequently, the amount for the available isolated Al sites within the zeolite framework (denoted as Al_{isol}) was obtained from the difference between those for the Al_{acce} and Al_{pair} sites,

$$n(\text{Al}_{\text{isol}}) = n(\text{Al}_{\text{acce}}) - n(\text{Al}_{\text{pair}}). \quad (1)$$



Scheme 1. Selective ion-exchanges of Na^+ and Co^{2+} ions with protons residing at isolated Al (Al_{isol}) and Al pair (Al_{pair}) sites of the zeolite framework.

Table 1 shows that the measured portions of Al_{acce} for the MOR-A, MOR-B, and MOR-C samples (with respect to the total Al content) are 57%, 31%, and 65%, respectively, which reflects the presence of extra-framework Al sites and the inaccessibility of a portion of the framework Al sites to the ion exchange because of steric hindrance. The $\text{Al}_{\text{pair}}/\text{Al}_{\text{isol}}$ ratios for these MOR samples follow an order of MOR-B (0.8) < MOR-C (2.4) < MOR-A (7.1), depending not only on the Si/Al ratio of the zeolites but also their supplier (MOR-A and MOR-C from Clariant, MOR-B from Nankai University Catalyst Co., Ltd.). Previous studies have found that the Al distribution of the aluminosilicate zeolites is very sensitive to the method and condition used in their synthesis [29–33], which may account for this observed trend of the $\text{Al}_{\text{pair}}/\text{Al}_{\text{isol}}$ ratio. As shown below, the diverse Al distributions of these MOR samples enable us to examine the influence of the different Al sites on the catalytic activity of Cu-exchanged aluminosilicate zeolites in methane oxidation.

Table 1. Si/Al ratios of parent H-MOR hosts and corresponding portions of framework Al sites accessible to $\text{Na}^+/\text{Co}^{2+}$ ion-exchanges ^a.

Sample	Si/Al	Al_{acce} (%) ^b	Al_{pair} (%) ^b	Al_{isol} (%) ^b	$\text{Al}_{\text{pair}}/\text{Al}_{\text{isol}}$
MOR-A	14	57	50	7	7.1
MOR-B	20	31	14	17	0.82
MOR-C	40	65	46	19	2.4

^a quantified by X-ray fluorescence spectroscopy and inductively coupled plasma optical emission spectrometry (details shown in the experimental section). ^b with respect to the total Al content.

Cu-MOR catalysts were prepared via a conventional aqueous ion-exchange method at a constant pH value of around 5.4 [16,17], during which Cu^{2+} ions can exchange with the protons associated with the accessible framework Al atoms. X-ray diffraction (XRD) patterns of these catalysts before or after methane oxidation were nearly identical to that of the parent MOR host (MOR-A used as an example in Figure 1a), indicating the framework of the MOR samples remained stable during the catalyst preparation and methane oxidation processes. The absence of diffraction peaks of Cu_2O or CuO phases in these XRD patterns suggests a high dispersion of Cu species bound to the MOR support, which is consistent with the fact that no CuO_x nanoparticles were detectable from the transmission electron microscopy (TEM) images of the Cu-MOR catalysts (Figure S1a of the supporting information). It is worth noting that if the precipitation of Cu^{2+} ions onto the external surface of the MOR support occurs, the resultant CuO_x particles can be readily observed via the TEM characterization as shown for the Cu-MOR-A sample prepared via the same ion-exchange process but at a slightly higher pH value (pH = 6.3; Figure S1b). Moreover, even at a Cu loading of $504 \mu\text{mol g}_{\text{cat}}^{-1}$, the surface area of the Cu-MOR catalyst declined only slightly compared to the parent MOR host (e.g., from 428 to $404 \text{ m}^2 \text{ g}_{\text{cat}}^{-1}$ for Cu-MOR-C; see Figure 1b). These results regarding the high dispersion of copper species were consistent with those reported previously [14,18].

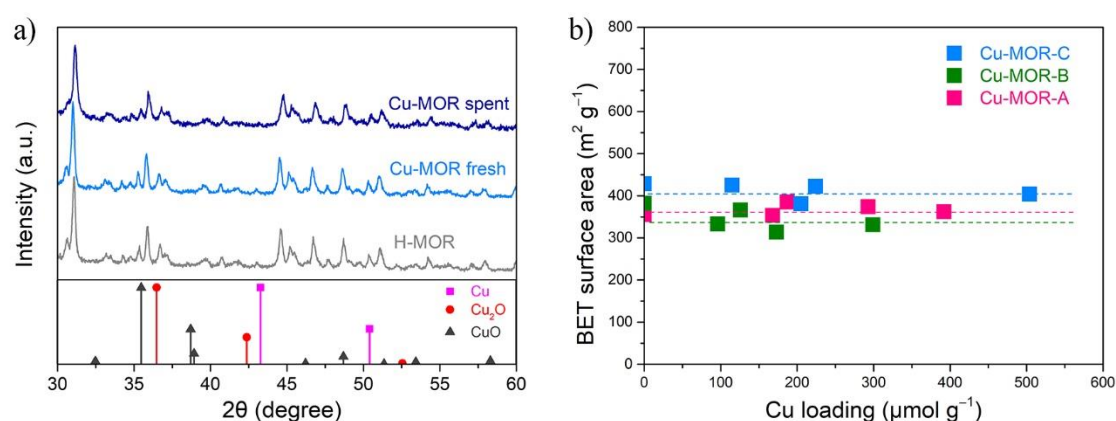


Figure 1. (a) Powder X-ray diffraction patterns for MOR and Cu-MOR samples (MOR-A, Si/Al = 14) with Cu (PDF-04-0836), Cu_2O (PDF-34-1354), and CuO (PDF-45-0937) as reference; (b) Surface area as a function of Cu loading for the Cu-MOR catalysts.

2.2. Reactivity of Cu-MOR Catalysts for Methane Oxidation

The activity of these Cu-MOR samples for the selective oxidation of methane was examined via a typical three-step reaction cycle widely applied [17], including (1) activation of the Cu-MOR catalysts in flowing O_2 at 723 K, (2) introduction of CH_4 onto the activated Cu-MOR catalysts at 473 K, and (3) extraction of CH_3OH from the Cu-MOR catalysts by steam flushing at 308 K (Figure 2a). No methanol product was observed in the effluent during the first two steps, and the methanol yield for each run was determined from the cumulative amount of CH_3OH over the entire period of the third step. It is also noteworthy that the concentration of CO_2 in the effluent was below the detection limit, which is consistent with the highly selective conversion of methane to methanol via this chemical looping manner [8–12].

Figure 2b shows the methanol yield as a function of the Cu loading of Cu-MOR-A. It was found that the normalized yield remained almost constant ($\approx 130 \text{ mmol mol}_{\text{Cu}}^{-1}$) at Cu loadings of $316 \mu\text{mol g}_{\text{cat}}^{-1}$ or less, corresponding to a Cu/ Al_{acce} ratio of 0.49 for the Cu-MOR-A sample. Then, the methanol yield decreased sharply to $44.8 \text{ mmol mol}_{\text{Cu}}^{-1}$ as the Cu loading further increased to $668 \mu\text{mol g}_{\text{cat}}^{-1}$, corresponding to a Cu/ Al_{acce} ratio of 1.0, which suggests that the protons of H-MOR-A were completely replaced by Cu^{2+} cations (in the form of $\text{Cu}(\text{OH})^+$ cations) during the aqueous ion-exchange preparation of

Cu-MOR catalysts. These results imply that Cu^{2+} species grafted on the AlO_4 tetrahedra units of H-MOR at low Cu loadings are different from those formed at high Cu loadings for methane oxidation, and the former is much more reactive. Considering that the MOR structures contain both eight-membered-ring (8-MR; 2.6×5.7 or 3.4×4.8 Å) and 12-membered-ring (12-MR; 6.5×7.0 Å) channels (Figure S2) and previous studies have shown that Cu^{2+} species grafted in the former voids exhibit higher activity in methane activation,^{8,17} we suppose that Cu^{2+} species prefer to exchange the protons residing in the 8-MR channels over those in the 12-MR ones as a consequence of the stronger dispersive stabilization in the smaller confining zeolite voids [35]. Similar effects of Cu loading on the normalized methanol yield were also observed for the Cu-MOR-B and Cu-MOR-C catalysts (Figure 2c,d), and their threshold loadings were close to 173 and 304 $\mu\text{mol g}_{\text{cat}}^{-1}$, respectively (corresponding to about 0.7 and 1.0 for their respective $\text{Cu}/\text{Al}_{\text{acce}}$ ratios).

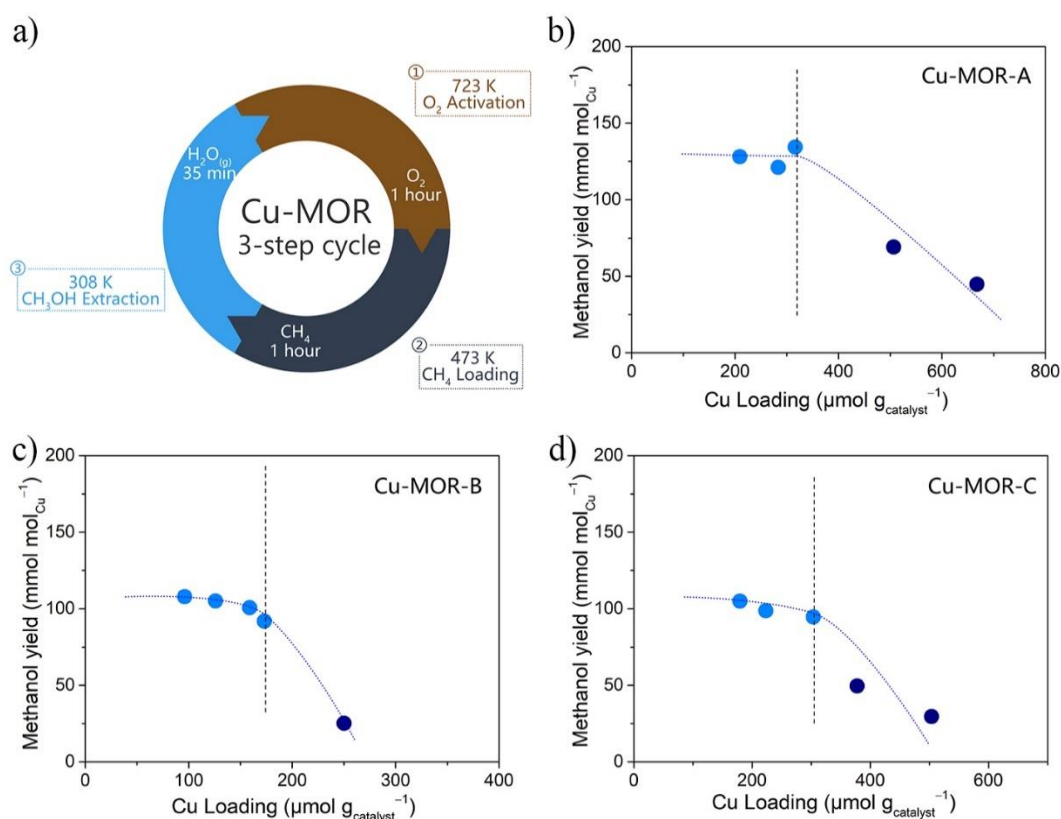


Figure 2. (a) The cyclic process of the methane-to-methanol reaction on Cu-MOR catalysts and the methanol yield (normalized by the exchanged Cu amount) as a function of Cu loading for (b) Cu-MOR-A, (c) Cu-MOR-B, and (d) Cu-MOR-C.

As shown in Figure 2, the methanol yields at the threshold Cu loading varied from 91.9 to 134.4 $\text{mmol mol}_{\text{Cu}}^{-1}$ for the three examined Cu-MOR samples, and the corresponding yields normalized by the total catalyst mass varied from 20.0 to 42.5 $\mu\text{mol g}_{\text{cat}}^{-1}$. It is notable that these productivity values were apparently lower than the highest one reported in the literature (200 $\mu\text{mol g}_{\text{cat}}^{-1}$) [12]. In addition to the effects of Si/Al ratio and zeolite framework, the lower productivity was likely due to the mild reaction condition applied (1 h of reaction time, 1.0 bar of methane partial pressure, 473 K), which was selected to mimic those previously used to study Cu-MOR catalysts.¹⁷ Recent studies have shown that a long reaction time and a high methane partial pressure are required for a complete reaction of the activated Cu-oxo species with methane [36,37]. Although the reaction conditions in our study were not optimal, the results obtained can still provide valuable information, because all of the methanol yields were evaluated under the same protocol.

The variation of the methanol yields at the threshold Cu loading shown in Figure 2 appears to reflect the distinct Al distributions among the three Cu-MOR samples, as discussed

above. Specifically, single $\text{Cu}(\text{OH})^+$ species grafted on the Al_{isol} sites can survive from the catalyst activation step at 723 K, while vicinal $\text{Cu}(\text{OH})^+$ species grafted on the Al_{pair} sites tend to form $\text{Cu}_2\text{O}_2^{2+}$, $\text{Cu}_3\text{O}_3^{2+}$, or even larger Cu-oxo clusters (illustrated in Figure S3). Although these Cu-containing moieties have been proposed as active sites for selective methane oxidation to methanol, their relative activities are still under debate [14–21]. As discussed next, in situ UV-Vis spectroscopic characterization of the activated Cu-MOR catalysts confirms that at least two types of Cu-containing moieties exist after the activation process (in flowing O_2 at 723 K) at low Cu loadings and they show distinct performances in methane oxidation.

The above discussion suggests that the methanol yield of the Cu-MOR samples is mainly due to the Cu-oxo species grafted in the 8-MR pockets, while those in the larger 12-MR channels are much less active. Assuming that the Al_{pair} and Al_{isol} sites are evenly distributed in the 8-MR and 12-MR voids, the $\text{Al}_{\text{pair}}/\text{Al}_{\text{isol}}$ ratio is used here as a convenient descriptor to discern the activity contributions of the Cu-containing moieties derived from these two types of sites. Figure 3 plots the methanol yields at the threshold Cu loading against the $\text{Al}_{\text{pair}}/\text{Al}_{\text{isol}}$ ratios for all the three Cu-MOR samples. The obtained positive correlation between the normalized methanol yield and the $\text{Al}_{\text{pair}}/\text{Al}_{\text{isol}}$ ratio clearly indicates that Cu_xO_y clusters formed on the Al_{pair} sites are preferred for methane activation, which is consistent with our theoretical assessment (shown below).

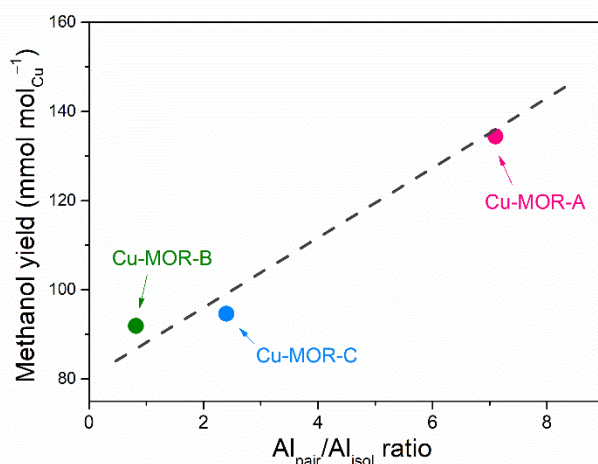


Figure 3. Correlation between $\text{Al}_{\text{pair}}/\text{Al}_{\text{isol}}$ ratios for the three Cu-MOR samples and their corresponding methanol yields at the threshold Cu loading. The dashed line represents a trend line.

2.3. In Situ UV-Vis Characterization of Methane Oxidation on Cu-MOR

In situ UV-Vis spectroscopy was employed here to examine the active sites of the Cu-MOR catalysts with their corresponding threshold Cu loadings. As shown in Figure 4a, a broad absorption band centered at $40,900 \text{ cm}^{-1}$ was observed for the Cu-MOR-A sample after the activation treatment in flowing O_2 at 723 K, which is ascribable to the charge transfer from $\text{O}^{2-}/\text{OH}^-$ to Cu^{2+} ions [17]. After contacting with CH_4 at 473 K for 1 h (i.e., the CH_4 loading step in Figure 2a), the intensity of this absorption band was reduced partially due to the consumption by methane oxidation, which is concomitant with a slight blue-shift of the band peak to $41,200 \text{ cm}^{-1}$. These phenomena suggest that the activated Cu-MOR samples contain at least two types of Cu-containing species, but the very broad feature of these UV-Vis bands hinders a rigorous deconvolution of the overlapping sub-bands. It is also noteworthy that these UV-Vis bands appear at wavenumbers apparently higher than those reported in the literature ($<38,000 \text{ cm}^{-1}$) [12,38], which may be derived from some systematic experimental shift toward higher wavenumbers.

To make a quantitative assessment, we assume that (1) the observed UV-Vis adsorption within the range of $20,000\text{--}50,000 \text{ cm}^{-1}$ is derived from two distinct types of Cu-containing species, and (2) both of the corresponding sub-bands have a Gaussian shape with their

peak positions unchanged for the Cu-MOR samples with different Si/Al ratios. Based on these hypotheses, we found that the optimized peak positions for the two sub-bands are 38,000 and 42,000 cm^{-1} , respectively, which allow excellent deconvolution for all the three Cu-MOR samples. With aid of the time-dependent density functional theory (Figures S4 and S5), we assigned the high-wavenumber band to the Cu-oxo clusters (e.g., Cu_2O_2 or Cu_3O_3) grafted at the Al_{pair} sites and the low-wavenumber one to the Cu-OH moiety grafted at the Al_{isol} sites. As shown in Figure 4b, the area ratio of the high-wavenumber band to the low-wavenumber one increased in the order of Cu-MOR-B (0.55) < Cu-MOR-C (0.77) < Cu-MOR-A (0.86), which is in line with the trend for the $\text{Al}_{\text{pair}}/\text{Al}_{\text{isol}}$ ratio of their parent MOR hosts (Table 1). These in situ UV-Vis spectra indicate again that the Cu-oxo clusters derived from the Al_{pair} sites of the zeolite framework are the preferred active species for methane activation. However, it needs to be emphasized that the conclusions drawn here are merely derived from the limited three series of Cu-MOR catalysts and thus still have uncertainty left.

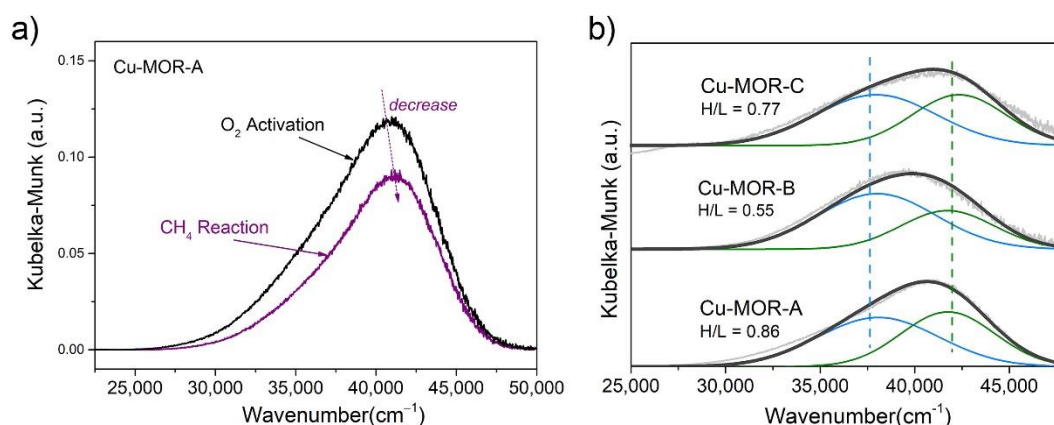


Figure 4. (a) In situ UV-Vis spectra of the activated Cu-MOR-A catalyst before and after the contact with methane at 473 K; (b) Fitting of the UV-Vis signals for the three Cu-MOR samples after O_2 activation with the area ratio of the high-wavenumber band to the low-wavenumber one (H/L) inserted. All the Cu-MOR samples used here are those with their respective threshold Cu loadings (shown in Figure 3).

2.4. Theoretical Assessment of Methane Oxidation on Cu-MOR

Periodic density functional theory (DFT) analysis was applied to compare the reactivity between the Cu-oxo clusters formed on the Al_{pair} sites and the CuOH group formed on the Al_{isol} sites. These Cu-containing species were built and optimized within the side pocket 8-MR of the MOR structure ($3.4 \times 4.8 \text{ \AA}$; Figure S2), which has been regarded as the preferred host void for methane oxidation [17,39]. Particularly, two types of Al_{isol} sites were considered here, as the corresponding CuOH groups bound to these Al_{isol} sites showed apparent difference in orientation (denoted as Cu1-a and Cu1-b; Figure 5a). For the case of Al_{pair} sites, two Si atoms of the 8-MR channel were replaced by Al atoms equivalently, and three types of Cu_2O_2 clusters were constructed based on the number of $(-\text{Si}-\text{O}-)$ units between the two inserted Al atoms in the resultant ring (denoted as Cu2- n , $n = 1-3$; Figure 5a). It is worth noting that the existence of $\text{Al}-\text{OH}-\text{Si}-\text{O}-\text{Al}-\text{OH}$ motif (i.e., Cu2-1) may have a very low possibility for the H-MOR samples used in our study because of their high Si/Al ratios (>14) [40–42], while Cu2-1 was still included here for the completeness of this theoretical assessment. A Cu_3O_3 cluster was also included for the $\text{Al}-\text{OH}-(\text{Si}-\text{O})_3-\text{Al}-\text{OH}$ motif (denoted as Cu3, Figure 5a), because several studies reported that such Cu_3O_3 clusters were uniquely reactive in methane oxidation [17,21].

Since the cleavage of the first C-H bond is generally the rate-determining step in methane activation [8,20,25], the reactivity of these Cu-containing species was evaluated via the dissociation energy of methane (ΔE_{diss}) that is defined as the energy change for

the dissociation of gaseous methane onto the Cu-MOR catalyst to form bound methyl and H-atom moieties:

$$\Delta E_{\text{diss}} = E_{\text{CH}_3^*+\text{H}^*} - E_{\text{Cu-MOR}} - E_{\text{CH}_4(\text{g})} \quad (2)$$

Here, $E_{\text{CH}_3^*+\text{H}^*}$ is the energy of the Cu-MOR catalyst with the bound methyl and H-atom species, whereas $E_{\text{Cu-MOR}}$ and $E_{\text{CH}_4(\text{g})}$ are the corresponding energies of the unreacted Cu-MOR catalyst and the gaseous methane. In particular, a recent theoretical study for methane oxidation [43] has shown that the activation barrier for the C-H bond cleavage in methane correlates linearly with the corresponding ΔE_{diss} values, indicating that this ΔE_{diss} term is an adequate descriptor for the reactivity of different Cu-oxo species on the C-H bond cleavage. It is also worth noting that the presence of these bound methyl and H-atom surface intermediates on Cu-MOR were confirmed via in situ diffuse reflectance infrared Fourier transform spectroscopy (DRIFTS) measurements (spectra shown in Figure S6).

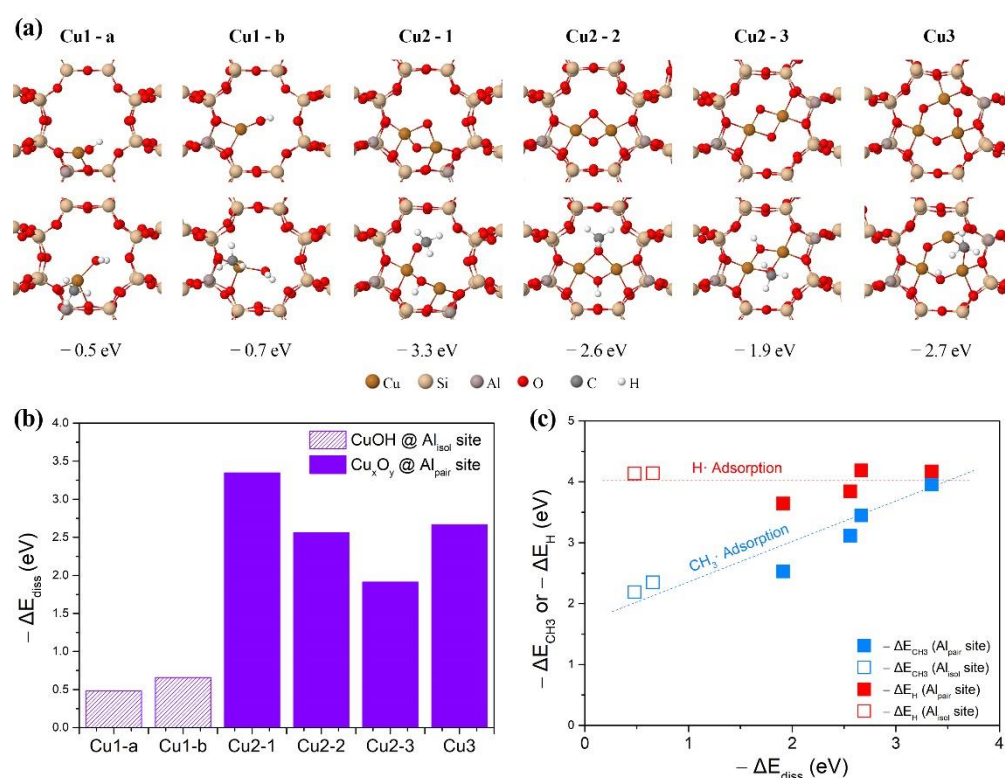


Figure 5. (a) DFT-derived structures of the original Cu-oxo species grafted at the 8-MR of MOR (above) and the corresponding structures after the dissociation of CH₄ onto the Cu-oxo species (below); (b) Calculated CH₄ dissociation energies (ΔE_{diss}) for the Cu-oxo clusters bound to the Al pair sites and the CuOH species bound to the isolated Al sites; (c) Correlation of the CH₄ dissociative adsorption energy (ΔE_{diss}) with the adsorption energies for the CH₃· (ΔE_{CH_3} , blue squares) and H· (ΔE_{H} , red squares) groups.

For methane activation on the CuOH species, our calculations showed that the dissociated methyl and H-atom prefer to locate at the Cu and O centers of the CuOH group, respectively (Figure S7), and the DFT-derived ΔE_{diss} values for Cu1-a and Cu1-b were similar with each other (−0.5 vs. −0.7 eV, Figure 5b). Compared with the CuOH species, the bi- μ -O nuclei of the Cu₂O₂ clusters can stabilize the dissociated methyl and H-atom moieties more efficiently, leading to much more negative ΔE_{diss} values (Cu2-1: −3.3 eV, Cu2-2: −2.6 eV, Cu2-3: −1.9 eV; Figure 5b). Similarly, a large value of −2.7 eV was obtained for ΔE_{diss} of the Cu₃O₃ clusters that possess tri- μ -O nuclei (Figure 5b). These calculated ΔE_{diss} numbers indicate that the Cu₂O₂ and Cu₃O₃ clusters derived from the Al_{pair} sites

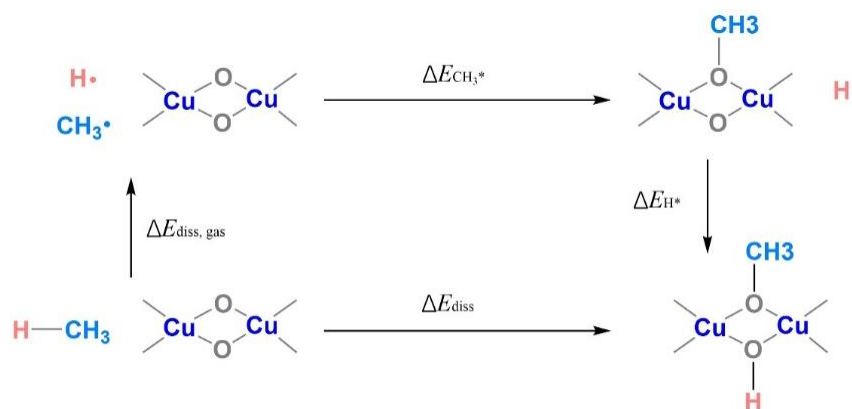
are apparently superior to the CuOH species derived from the Al_{isol} sites in methane activation, which is consistent with the experimental findings shown above.

It should be noted that ΔE_{diss} for the Cu₂O₂ clusters is sensitive to the distance between the two Al_{pair} sites in the 8MR. Geometrical analysis of the Cu₂O₂ clusters shows that as the number of the (–Si–O–) units between the two Al atoms increased from 1 to 3, the averaged Cu–O–Cu bond angle increased from 88.8° to 99.0°, while the Cu–O bond length changed only slightly from 1.811 to 1.790 Å (Table S1). Consequently, the tensile force of the Cu₂O₂ ring decreased as the two Al atoms became farther away in the 8-MR, making the Cu₂O₂ clusters less active in methane dissociation.

In attempt to capture the key factors that determine the reactivity of Cu-MOR catalysts for methane activation, a thermochemical cycle was designed to analyze the methane dissociation on Cu-containing species. As shown in Scheme 2, ΔE_{diss} can be decomposed into the energy required for the dissociation of methane to form CH₃· and H· radicals in the gas phase ($\Delta E_{\text{diss,gas}}$) and the energies released from the bonding of the CH₃· and H· radicals onto the Cu-containing species ($\Delta E_{\text{CH}_3^*}$ and ΔE_{H^*} , respectively).

$$\Delta E_{\text{diss}} = \Delta E_{\text{diss,gas}} + \Delta E_{\text{CH}_3^*} + \Delta E_{\text{H}^*} \quad (3)$$

Specifically, the value of $\Delta E_{\text{diss,gas}}$ merely reflects the intrinsic strength of the C–H bond in methane, whereas $\Delta E_{\text{CH}_3^*}$ and ΔE_{H^*} are those factors relevant to the catalytic reactivity. Figure 5c depicts the $\Delta E_{\text{CH}_3^*}$ and ΔE_{H^*} values as functions of ΔE_{diss} for all the examined CuOH and Cu-oxo species. It is apparent that ΔE_{H^*} is nearly insensitive to ΔE_{diss} , while a good correlation is obtained between $\Delta E_{\text{CH}_3^*}$ and ΔE_{diss} . In other words, how to stabilize the methyl moiety on the confined Cu-containing sites is critical in determining the reactivity of Cu–MOR catalysts. As shown above, the stabilization of the methyl moiety can be improved by tuning the electronic property of μ -O nuclei or increasing the tensile force of the Cu–O–Cu bond.



Scheme 2. Thermochemical cycle analysis for the dissociation of methane on Cu-containing species grafted in MOR (Cu₂O₂ clusters used here as an example).

3. Methods

3.1. Catalyst Preparation

Cu-exchanged mordenite (Cu-MOR) catalysts with different Cu loadings were prepared via a conventional aqueous ion-exchange method [17]. Before the ion-exchange process, commercial H-MOR zeolites (two H-MOR samples with Si/Al ratios of 14 and 40 purchased from Clariant; one H-MOR sample with a Si/Al ratio of 20 purchased from Nankai University Catalyst Co., Ltd.) were pre-treated in a muffle furnace under stagnant ambient air by ramping the temperature from ambient to 773 K at 1 K s^{−1} and holding for 5 h. The Cu²⁺ exchange was carried out at ambient temperature by mixing 2.0 g zeolite with 120 mL of aqueous Cu(CH₃COO)₂ (AR, Xilong Scientific Co., Ltd., Guangdong, China) solution. The Cu(CH₃COO)₂ concentration of the solution was varied between 0.0025 and

0.025 mol L⁻¹ to obtain copper loadings of 0.1–0.7 mmol g⁻¹. During this ion-exchange process, the pH value of the aqueous solution was controlled to around 5.4 via adding a diluted NH₄OH solution (Sinopharm Group Co., Ltd., Shanghai, China). After the ion exchange for 24 h, the resultant solid was separated via centrifugation and washed by deionized water four times. Then, these samples were dried in static ambient air at 373 K overnight. The calcination and activation of these Cu-exchanged catalysts were conducted in following O₂ at 723 K in situ during the stepwise oxidation of methane to methanol as described in Section 3.3.

3.2. Catalyst Characterization

The crystal structures of catalysts were determined from the powder X-ray diffraction (XRD) patterns collected in Rigaku D/MAX-rC (Cu-K_α radiation, λ = 1.5418 Å, 35 kV, 15 mA, Tokyo, Japan). The data were recorded by increasing the 2θ value from 5° to 60° (10° min⁻¹). The morphology of Cu-MOR was examined on the Tecnai G2 F20 transmission electron microscope (TEM; FEI, USA) operating at 200 kV. The concentrations of Cu, Al, and Si elements in the Cu-MOR catalysts were quantified by X-ray Fluorescence Spectrometer (XRF) using BRUKER S8 TIGER (60 kV, 40 mA, 1084 mbar, 2.0 mL min⁻¹, MA, USA), while the surface area of the solid samples was measured on Micromeritics Tristar 2020 (GA, USA) at 78 K after a thermal pretreatment (513 K, 4 h, vacuum). The aluminum distribution of the examined MOR zeolites was probed by Na⁺ and Co²⁺ ion-exchange methods, since these two ions can selectively exchange the protons derived from the different Al sites in the zeolite framework [17,31]. Specifically, the Na⁺-exchange of the H-MOR zeolites was conducted in a 0.05 mol L⁻¹ NaNO₃ solution for 24 h at 333 K, which was followed by drying at 373 K for 24 h. The Co²⁺-exchange of the resultant Na-MOR samples was conducted in a 0.05 mol L⁻¹ Co(NO₃)₂ solution at ambient temperature 3 times, and each time, it lasted for 12 h. The concentrations of Na and Co elements in the exchanged samples were determined by the inductively coupled plasma optical emission spectrometry (ICP, Thermo Fisher Scientific, Waltham, MA, USA, ICP7400).

3.3. Testing of Activity for Methane Oxidation to Methanol

The activity of Cu-MOR catalysts was evaluated in a U-shaped quartz reactor with an inner diameter of 8 mm. The reaction process consisted of three sequential steps, including activation by O₂, reaction with CH₄, and extraction with H₂O stream. In a typical experiment, 0.2 g Cu-MOR (250–380 μm) was treated in flowing O₂ (16 mL min⁻¹) at 723 K for 1 h and then cooled down to 473 K. After purging in He, the sample was treated in 90% CH₄/He (19 mL min⁻¹) at 473 K for 1 h and then cooled to 308 K and purged in He. In the last step, a mixture of H₂O stream (14 mL min⁻¹) and He (10 mL min⁻¹) passed through the catalyst bed for 35 min. These reaction parameters were adopted from those previously used to study Cu-MOR catalysts¹⁷ and were not further optimized. The reaction products were detected and quantified by an online mass spectroscopy (OmniStarTM/ThermoStarTM GSD320 Gas Analysis System, Headquarters, Germany) through monitoring the signals at *m/z* ratios of 31, 44, and 46, which were ascribed to the formed CH₃OH, CO₂, and (CH₃O)₂O species, respectively.

3.4. Ultraviolet-Visible Spectroscopy Measurements

Ultraviolet-visible (UV-Vis) spectra were acquired on Agilent Cary 100 (Santa Clara, CA, USA) in the range from 20,000 to 50,000 cm⁻¹ at 15,000 cm⁻¹ min⁻¹. The gaseous environment during the UV-Vis measurement was identical to the process for the activity testing. The signal of each fresh catalyst was collected as the respective baseline. The intensity of the diffuse reflectance UV-Vis spectra was presented in the form of the Kubelka–Munk function as given by

$$F(R) = (1 - R)^2 \div (2 \times R) \quad (4)$$

where R is the ratio of the reflectance of the sample in reaction to the reflectance of the fresh sample.

3.5. Periodic Density Functional Theory Treatments

The periodic density functional theory (DFT) calculations of adsorption energy within the MOR structure ($a = 18.09 \text{ \AA}$, $b = 20.52 \text{ \AA}$, $c = 7.52 \text{ \AA}$; modeled with a $1 \times 1 \times 2$ unit cell) were carried out using Vienna ab initio simulation package (VASP, version 5.4.1) [44–47]. The electron exchange–correlation was treated by the generalized gradient approximation (GGA) based on the Perdew–Burke–Ernzerhof (PBE) functional [48], and van der Waals correction was included using the Grimme’s D3BJ method [49]. The plane wave basis set was truncated with a cutoff energy of 400 eV. The Brillouin zone was sampled using the gamma point, whereas the Gaussian smearing was set at 0.05 eV. All atoms were allowed to relax during geometry optimizations until the maximum force on each atom was less than 0.05 eV \AA^{-1} .

4. Conclusions

The quantification of isolate Al sites and Al pair sites within the MOR zeolite host by conventional $\text{Na}^+/\text{Co}^{2+}$ aqueous ion-exchange methods provides an effective approach to discern the reactivity difference between the Cu-containing species derived from the accessible framework Al sites for methane oxidation to methanol. Particularly, the most reactive Cu-containing species for the Cu-MOR catalysts are those formed at low Cu loadings, which plausibly reside in the 8-MR channels instead of the 12-MR ones. A good correlation between the methanol yield (normalized by the Cu amount) at low Cu loadings and the ratio of the Al pair sites to the isolate Al sites suggests that the observed activity of Cu-MOR in methane oxidation is mainly ascribed to the Cu-oxo clusters grafted at the Al pair sites. In situ UV-Vis spectroscopic measurements and DFT calculations further support that these Cu-oxo clusters are more reactive than the CuOH species bound to the isolated Al sites. By applying a theoretical analysis on the energetics of the first C–H bond cleavage in methane, it is unveiled that the stabilization of the formed methyl moiety onto the Cu-containing species determines the reactivity of methane oxidation, and the bridged-O centers within the Cu-oxo clusters are favored to hold the methyl moieties, which accounts for the higher reactivity of these Cu-oxo clusters than the CuOH species.

Supplementary Materials: The following are available online at <https://www.mdpi.com/article/10.3390/catal11060751/s1>, Figure S1: TEM images for the Cu-MOR-A catalyst ($424 \mu\text{molCu}_{\text{gcatalyst}}^{-1}$) prepared at constant pH values of (a) 5.4 and (b) 6.3; Figure S2: Illustration of the 12-MR and 8-MR motifs in MOR; Figure S3: Formation of Cu_2O_2 clusters from two vicinal CuOH species bound to Al pair sites in MOR; Figure S4: Predicted UV-Vis spectra of the MOR-supported Cu-oxo species before (solid) and after (dotted) reaction with methane; Figure S5: Predicted UV-Vis spectra of the MOR zeolite structure; Figure S6; in situ Diffuse reflectance infrared Fourier transform spectra for an activated Cu-MOR-A sample after the methane oxidation process at 473 K for 1 h; Figure S7: DFT-derived structures for Cu1-b bound with dissociated methyl and H moieties and the corresponding dissociation energy of methane; Table S1: DFT-derived geometric parameters and charge distribution for the Cu-oxo species before and after methane dissociation onto them.

Author Contributions: Y.W. and S.W. (Shuai Wang) conceived the idea for the project. P.H., Z.Z. and Z.C. conducted the catalyst synthesis and performed the catalytic tests. P.H. conducted the theoretical calculations. P.H. drafted the manuscript under the guidance of S.W. (Shuai Wang), J.L., S.W. (Shaolong Wan) and Y.W. All authors discussed and commented on the manuscript.

Funding: This work was supported by the National Natural Science Foundation of China (No. 91945301, 21922201, 21872113, and 91545114) and the Fundamental Research Funds for the Central Universities (No. 20720190036).

Conflicts of Interest: There are no conflict to declare.

References

1. Meng, X.; Cui, X.; Rajan, N.P.; Yu, L.; Deng, D.; Bao, X. Direct Methane Conversion under Mild Condition by Thermo-, Electro-, or Photocatalysis. *Chem* **2019**, *5*, 2296–2325. [[CrossRef](#)]
2. Saha, D.; Grappe, H.A.; Chakraborty, A.; Orkoulas, G. Postextraction Separation, On-Board Storage, and Catalytic Conversion of Methane in Natural Gas: A Review. *Chem. Rev.* **2016**, *116*, 11436–11499. [[CrossRef](#)]
3. Sun, L.; Wang, Y.; Guan, N.; Li, L. Methane Activation and Utilization: Current Status and Future Challenges. *Energy Technol.* **2019**, *8*, 1900826. [[CrossRef](#)]
4. Bao, J.; Yang, G.; Yoneyama, Y.; Tsubaki, N. Significant Advances in C1 Catalysis: Highly Efficient Catalysts and Catalytic Reactions. *ACS Catal.* **2019**, *9*, 3026–3053. [[CrossRef](#)]
5. Lian, M.; Wang, Y.; Zhao, M.; Li, Q.; Weng, W.; Xia, W.; Wan, H. Stability of Ni/SiO₂ in Partial Oxidation of Methane: Effects of W Modification. *Acta Phys. Chim. Sin.* **2019**, *35*, 607–615. [[CrossRef](#)]
6. Jin, Z.; Wang, L.; Zuidema, E.; Mondal, K.; Zhang, M.; Zhang, J.; Wang, C.; Meng, X.; Yang, H.; Mesters, C.; et al. Hydrophobic Zeolite Modification for in situ Peroxide Formation in Methane Oxidation to Methanol. *Science* **2020**, *367*, 193–197. [[CrossRef](#)]
7. Sun, L.; Wang, Y.; Wang, C.; Xie, Z.; Guan, N.; Li, L. Water-Involved Methane-Selective Catalytic Oxidation by Dioxygen over Copper Zeolites. *Chem* **2021**, *7*, 1557–1568. [[CrossRef](#)]
8. Ravi, M.; Ranocchiari, M.; van Bokhoven, J.A. The Direct Catalytic Oxidation of Methane to Methanol—A Critical Assessment. *Angew. Chem. Int. Ed.* **2017**, *56*, 16464–16483. [[CrossRef](#)]
9. Tomkins, P.; Ranocchiari, M.; van Bokhoven, J.A. Direct Conversion of Methane to Methanol under Mild Conditions over Cu-Zeolites and beyond. *Acc. Chem. Res.* **2017**, *50*, 418–425. [[CrossRef](#)] [[PubMed](#)]
10. Snyder, B.E.R.; Bols, M.L.; Schoonheydt, R.A.; Sels, B.F.; Solomon, E.I. Iron and Copper Active Sites in Zeolites and Their Correlation to Metalloenzymes. *Chem. Rev.* **2018**, *118*, 2718–2768. [[CrossRef](#)]
11. Mahyuddin, M.H.; Shiota, Y.; Yoshizawa, K. Methane selective oxidation to methanol by metal-exchanged zeolites: A review of active sites and their reactivity. *Catal. Sci. Technol.* **2019**, *9*, 1744–1768. [[CrossRef](#)]
12. Newton, M.A.; Knorpp, A.J.; Sushkevich, V.L.; Palagin, D.; van Bokhoven, J.A. Active sites and mechanisms in the direct conversion of methane to methanol using Cu in zeolitic hosts: A critical examination. *Chem. Soc. Rev.* **2020**, *49*, 1449–1486. [[CrossRef](#)] [[PubMed](#)]
13. Que, L., Jr.; Tolman, W.B. Biologically inspired oxidation catalysis. *Nature* **2008**, *455*, 333–340. [[CrossRef](#)] [[PubMed](#)]
14. Bozbag, S.E.; Alayon, E.M.C.; Pechacek, J.; Nachtegaal, M.; Ranocchiari, M.; van Bokhoven, J.A. Methane to methanol over copper mordenite: Yield improvement through multiple cycles and different synthesis techniques. *Catal. Sci. Technol.* **2016**, *6*, 5011–5022. [[CrossRef](#)]
15. Groothaert, M.H.; Smeets, P.J.; Sels, B.F.; Jacobs, P.A.; Schoonheydt, R.A. Selective oxidation of methane by the bis(mu-oxo)dicopper core stabilized on ZSM-5 and mordenite zeolites. *J. Am. Chem. Soc.* **2005**, *127*, 1394–1395. [[CrossRef](#)] [[PubMed](#)]
16. Grundner, S.; Luo, W.; Sanchez-Sanchez, M.; Lercher, J.A. Synthesis of single-site copper catalysts for methane partial oxidation. *Chem. Commun.* **2016**, *52*, 2553–2556. [[CrossRef](#)] [[PubMed](#)]
17. Grundner, S.; Markovits, M.A.; Li, G.; Tromp, M.; Pidko, E.A.; Hensen, E.J.; Jentys, A.; Sanchez-Sanchez, M.; Lercher, J.A. Single-site trinuclear copper oxygen clusters in mordenite for selective conversion of methane to methanol. *Nat. Commun.* **2015**, *6*, 7546. [[CrossRef](#)]
18. Le, H.V.; Parishan, S.; Sagaltchik, A.; Gobel, C.; Schlesiger, C.; Malzer, W.; Trunschke, A.; Schomacker, R.; Thomas, A. Solid-State Ion-Exchanged Cu/Mordenite Catalysts for the Direct Conversion of Methane to Methanol. *ACS Catal.* **2017**, *7*, 1403–1412. [[CrossRef](#)]
19. Narsimhan, K.; Iyoki, K.; Dinh, K.; Roman-Leshkov, Y. Catalytic Oxidation of Methane into Methanol over Copper-Exchanged Zeolites with Oxygen at Low Temperature. *ACS Cent. Sci.* **2016**, *2*, 424–429. [[CrossRef](#)]
20. Sushkevich, V.L.; Palagin, D.; Ranocchiari, M.; van Bokhoven, J.A. Selective anaerobic oxidation of methane enables direct synthesis of methanol. *Science* **2017**, *356*, 523–527. [[CrossRef](#)]
21. Sushkevich, V.L.; Palagin, D.; van Bokhoven, J.A. The Effect of the Active-Site Structure on the Activity of Copper Mordenite in the Aerobic and Anaerobic Conversion of Methane into Methanol. *Angew. Chem. Int. Ed.* **2018**, *57*, 8906–8910. [[CrossRef](#)]
22. Wang, G.R.; Chen, W.; Huang, L.; Liu, Z.Q.; Sun, X.Y.; Zheng, A.M. Reactivity descriptors of diverse copper-oxo species on ZSM-5 zeolite towards methane activation. *Catal. Today* **2019**, *338*, 108–116. [[CrossRef](#)]
23. Woertink, J.S.; Smeets, P.J.; Groothaert, M.H.; Vance, M.A.; Sels, B.F.; Schoonheydt, R.A.; Solomon, E.I. A [Cu₂O]²⁺ core in Cu-ZSM-5, the active site in the oxidation of methane to methanol. *Proc. Natl. Acad. Sci. USA* **2009**, *106*, 18908–18913. [[CrossRef](#)]
24. Pappas, D.K.; Borfecchia, E.; Dyballa, M.; Pankin, I.A.; Lomachenko, K.A.; Martini, A.; Signorile, M.; Teketel, S.; Arstad, B.; Berlier, G.; et al. Methane to Methanol: Structure-Activity Relationships for Cu-CHA. *J. Am. Chem. Soc.* **2017**, *139*, 14961–14975. [[CrossRef](#)]
25. Kulkarni, A.R.; Zhao, Z.-J.; Siahrostami, S.; Nørskov, J.K.; Studt, F. Monocopper Active Site for Partial Methane Oxidation in Cu-Exchanged 8MR Zeolites. *ACS Catal.* **2016**, *6*, 6531–6536. [[CrossRef](#)]
26. Knorpp, A.; Pinar, A.B.; Baerlocher, C.; McCusker, L.B.; Casati, N.; Newton, M.A.; Checchia, S.; Meyet, J.; Palagin, D.; van Bokhoven, J.A. Paired copper monomers in zeolite omega: The active site for methane-to-methanol conversion. *Angew. Chem. Int. Ed.* **2021**, *60*, 5854–5858. [[CrossRef](#)]

27. Mahyuddin, M.H.; Tanaka, T.; Shiota, Y.; Staykov, A.; Yoshizawa, K. Methane Partial Oxidation over $[\text{Cu}_2(\mu\text{-O})]^{2+}$ and $[\text{Cu}_3(\mu\text{-O})_3]^{2+}$ Active Species in Large-Pore Zeolites. *ACS Catal.* **2018**, *8*, 1500–1509. [[CrossRef](#)]
28. Palagin, D.; Knorpp, A.J.; Pinar, A.B.; Ranocchiari, M.; van Bokhoven, J.A. Assessing the relative stability of copper oxide clusters as active sites of a CuMOR zeolite for methane to methanol conversion: Size matters? *Nanoscale* **2017**, *9*, 1144–1153. [[CrossRef](#)] [[PubMed](#)]
29. Dědeček, J.; Kaucký, D.; Wichterlová, B. Co^{2+} ion siting in pentasil-containing zeolites, part 3. *Microporous Mesoporous Mater.* **2000**, *35–36*, 483–494. [[CrossRef](#)]
30. Dědeček, J.; Kaucký, D.; Wichterlová, B. Al distribution in ZSM-5 zeolites: An experimental study. *Chem. Commun.* **2001**, 970–971. [[CrossRef](#)]
31. Dědeček, J.; Kaucký, D.; Wichterlová, B.; Gonsiorová, O. Co^{2+} ions as probes of Al distribution in the framework of zeolites. ZSM-5 study. *Phys. Chem. Chem. Phys.* **2002**, *4*, 5406–5413. [[CrossRef](#)]
32. Karcz, R.; Dedecek, J.; Supronowicz, B.; Thomas, H.M.; Klein, P.; Tabor, E.; Sazama, P.; Pashkova, V.; Sklenak, S. TNU-9 Zeolite: Aluminum Distribution and Extra-Framework Sites of Divalent Cations. *Chem. Eur. J.* **2017**, *23*, 8857–8870. [[CrossRef](#)] [[PubMed](#)]
33. Mlekodaj, K.; Dedecek, J.; Pashkova, V.; Tabor, E.; Klein, P.; Urbanova, M.; Karcz, R.; Sazama, P.; Whittleton, S.R.; Thomas, H.M.; et al. Al Organization in the SSZ-13 Zeolite. Al Distribution and Extraframework Sites of Divalent Cations. *J. Phys. Chem. C* **2018**, *123*, 7968–7987. [[CrossRef](#)]
34. Indovina, V.; Campa, M.C.; Pietrogiamici, D. Isolated Co^{2+} and $[\text{Co}-\text{O}-\text{Co}]^{2+}$ Species in Na-MOR Exchanged with Cobalt to Various Extents: An FTIR Characterization by CO Adsorption of Oxidized and Prereduced Samples. *J. Phys. Chem. C* **2008**, *112*, 5093–5101. [[CrossRef](#)]
35. Gounder, R.; Iglesia, E. The catalytic diversity of zeolites: Confinement and solvation effects within voids of molecular dimensions. *Chem. Commun.* **2013**, *49*, 3491–3509. [[CrossRef](#)]
36. Tomkins, P.; Mansouri, A.; Bozbag, S.E.; Krumeich, F.; Park, M.B.; Alayon, E.M.C.; Ranocchiari, M.; van Bokhoven, J.A. Isothermal cyclic conversion of methane into methanol over copper-exchanged zeolite at low temperature. *Angew. Chem. Int. Ed.* **2016**, *55*, 5467–5471. [[CrossRef](#)]
37. Brezicki, G.; Kammert, J.D.; Gunnoe, T.B.; Paolucci, C.; Davis, R.J. Insights into the speciation of Cu in the Cu-H-mordenite catalyst for the oxidation of methane to methanol. *ACS Catal.* **2019**, *9*, 5308–5319. [[CrossRef](#)]
38. Ikuno, T.; Grundner, S.; Jentys, A.; Li, G.; Pidko, E.; Fulton, J.; Sanchez-Sanchez, M.; Lercher, J.A. Formation of Active Cu-oxo Clusters for Methane Oxidation in Cu-Exchanged Mordenite. *J. Phys. Chem. C* **2019**, *123*, 8759–8769. [[CrossRef](#)]
39. Vanelderen, P.; Snyder, B.E.; Tsai, M.L.; Hadt, R.G.; Vancauwenbergh, J.; Coussens, O.; Schoonheydt, R.A.; Sels, B.F.; Solomon, E.I. Spectroscopic definition of the copper active sites in mordenite: Selective methane oxidation. *J. Am. Chem. Soc.* **2015**, *137*, 6383–6392. [[CrossRef](#)]
40. Dědeček, J.; Sklenak, S.; Li, C.; Wichterlová, B.; Gábová, V.; Brus, J.; Sierka, M.; Sauer, J. Effect of Al–Si–Al and Al–Si–Si–Al Pairs in the ZSM-5 Zeolite Framework on the ^{27}Al NMR Spectra. A Combined High-Resolution ^{27}Al NMR and DFT/MM Study. *J. Phys. Chem. C* **2009**, *113*, 1447–1458. [[CrossRef](#)]
41. Takaishi, T.; Kato, M.; Itabashi, K. Determination of the ordered distribution of aluminum atoms in a zeolitic framework. Part II. *Zeolites* **1995**, *15*, 21–32. [[CrossRef](#)]
42. Takaishi, T.; Kato, M.; Itabashi, K. Stability of the Al–O–Si–O–Al Linkage in a Zeolitic Framework. *J. Phys. Chem.* **1994**, *98*, 5742–5743. [[CrossRef](#)]
43. Arvidsson, A.A.; Zhdanov, V.P.; Carlsson, P.-A.; Grönbeck, H.; Hellman, A. Metal dimer sites in ZSM-5 zeolite for methane-to-methanol conversion from first-principles kinetic modelling: Is the $[\text{Cu}-\text{O}-\text{Cu}]^{2+}$ motif relevant for Ni, Co, Fe, Ag, and Au? *Catal. Sci. Technol.* **2017**, *7*, 1470–1477. [[CrossRef](#)]
44. Kresse, G.; Hafner, J. Ab initio molecular dynamics for open-shell transition metals. *Phys. Rev. B Condens. Matter* **1993**, *48*, 13115–13118. [[CrossRef](#)]
45. Kresse, G.; Hafner, J. Ab initio molecular-dynamics simulation of the liquid-metal-amorphous-semiconductor transition in germanium. *Phys. Rev. B Condens. Matter* **1994**, *49*, 14251–14269. [[CrossRef](#)]
46. Kresse, G.; Furthmüller, J. Efficiency of ab-initio total energy calculations for metals and semiconductors using a plane-wave basis set. *Comput. Mater. Sci.* **1996**, *6*, 15–50. [[CrossRef](#)]
47. Kresse, G.; Furthmüller, J. Efficient iterative schemes for ab initio total-energy calculations using a plane-wave basis set. *Phys. Rev. B Condens. Matter* **1996**, *54*, 11169–11186. [[CrossRef](#)] [[PubMed](#)]
48. Perdew, J.P.; Burke, K.; Ernzerhof, M. Generalized Gradient Approximation Made Simple. *Phys. Rev. Lett.* **1996**, *77*, 3865–3868. [[CrossRef](#)]
49. Grimme, S. Semiempirical GGA-type density functional constructed with a long-range dispersion correction. *J. Comput. Chem.* **2006**, *27*, 1787–1799. [[CrossRef](#)] [[PubMed](#)]